Type of file: figure
Label: SupFig1
Filename: Supplementary Figure 1.doc

**Supplementary Figure 1: Flow chart illustrating the initial microRNA binding site identification steps.**

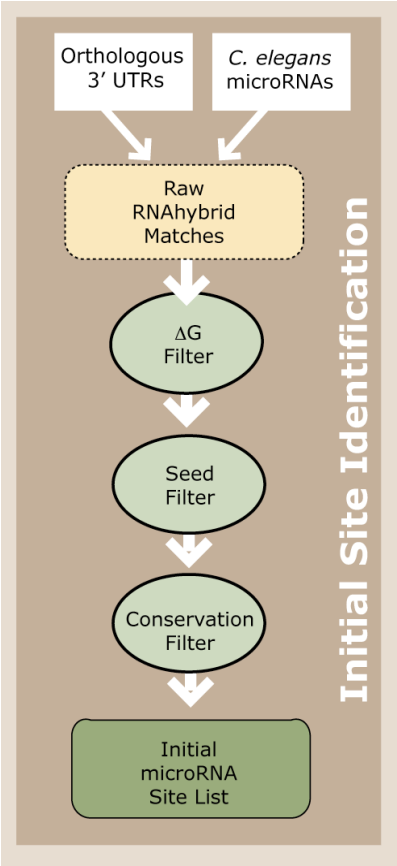


**Figure S1: Flow chart illustrating the initial microRNA binding site identification steps.** As described in the Supplemental Results and Supplemental Methods sections, we began by running RNAhybrid using all C. elegans 3' UTR and microRNA sequences as input. We then implemented several liberal filters to reduce noise. These included: (1) a threshold on the hybrid interaction energy, DG, (2) a limit on the G:U wobble pairs and bulges allowed within the seed region and (3) a conservation filter requiring that the above two filters be passed in orthologous *C. elegans* and *C. briggsae* 3' UTRs. Details on these filters are given in the text of Supplemental Methods. The resulting list of binding sites formed the input for all of the subsequent analysis (see Figure 1).

Type of file: figure
Label: SupFig2
Filename: Supplementary Figure 2.doc

**Supplementary Figure 2: Contextual Features Not Correlated with Enrichment for AIN-IP Transcripts.**

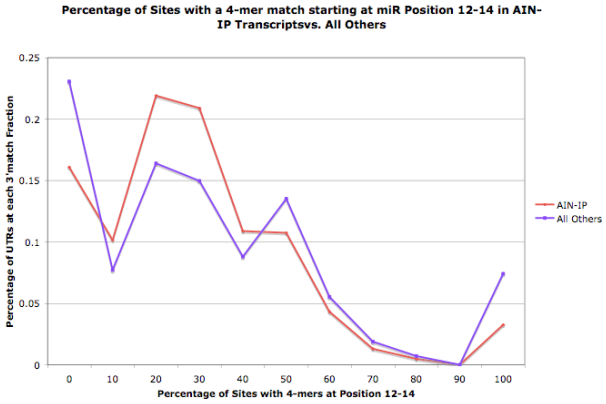


**Fig 2 a**

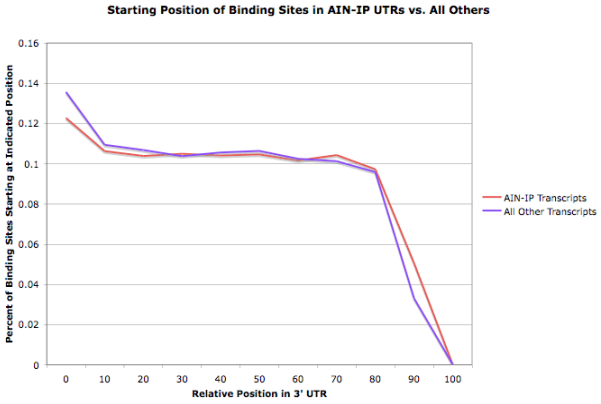


**Fig 2 b**

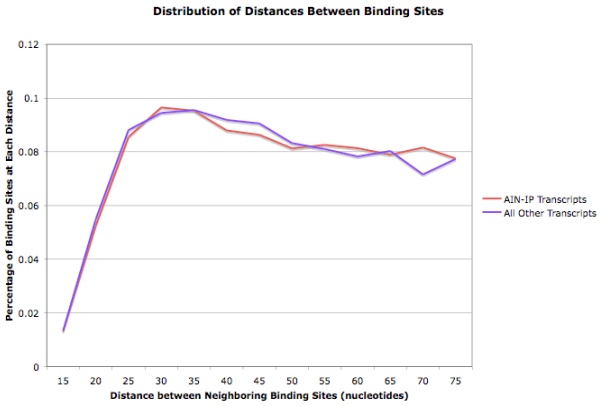


**Fig 2 c**

**Supplementary Figure 2: Contextual Features Not Correlated with Enrichment for AIN-IP Transcripts.** We evaluated several other features that have been proposed to correlate with efficacy of regulation in tissue culture transfection experiments (Grimson et al., 2007 [3]). **A**. A sliding window of 4 nucleotides was used to look for blocks of pairing at the 3' end of the miRNA::target duplex, across from nucleotides 12-14 of the miRNA. No significant enrichment for 3' pairing was seen for AIN-IP transcripts. **B**. AIN-IP transcripts show a slight bias for starting positions near the stop codon, but this bias is not significantly different from that seen in all other transcripts. **C**. All transcripts show a deficit in the number of binding sites that lie within about 25 nucleotides of each other, with no significant difference between AIN-IP transcripts and all others.

Type of file: figure
Label: SupFig3
Filename: Supplementary Figure 3.doc

**Supplementary Figure 3: ROC curves used to optimize mirWIP method**

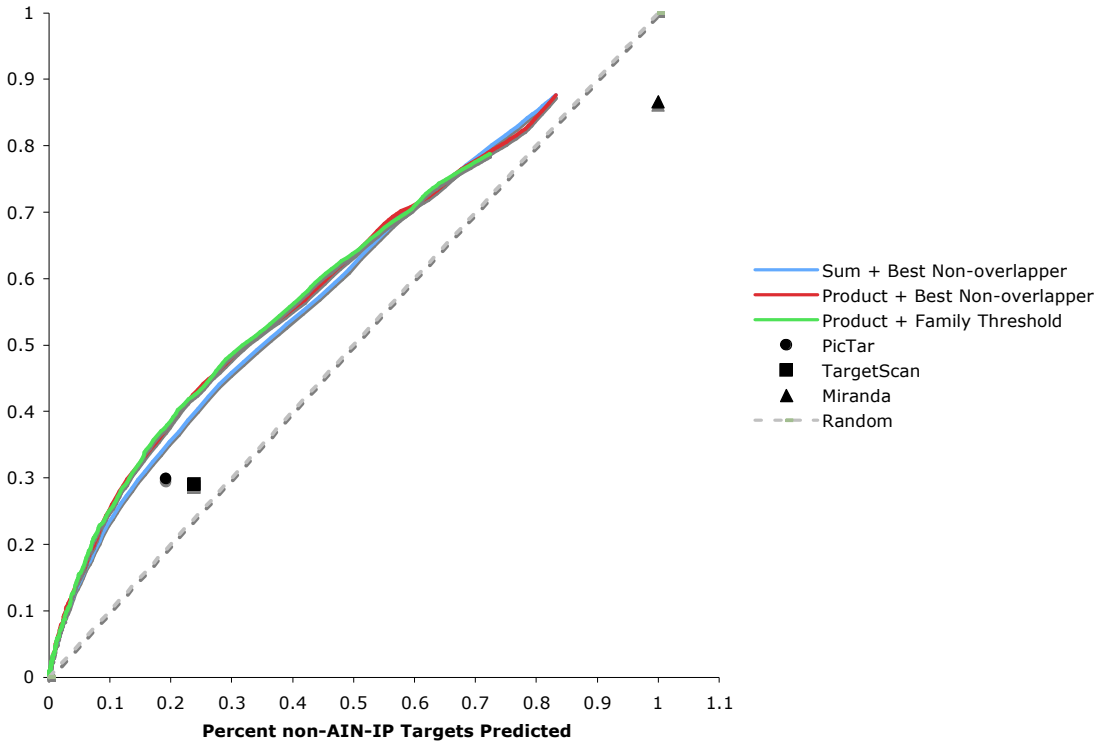


**Supplementary Figure 3: ROC curves used to optimize mirWIP method.** We optimized our algorithm using to two measures: (1) ability to return verified targets as shown in the main text and (2) ability to separate AIN-IP from non-AIN-IP targets as shown in the receiver operator characteristic (ROC) curve above. We had the option of including the enrichment factors as a linear sum of weights (blue line) or as a product of weights (red and green lines). We also had the option of choosing the best non-overlapping site or the best non-overlapping family member. For reference, we also included the performance of three highly cited methods from other groups and a random selection curve. Each mode of the mirWIP algorithm outperformed these standard methods, but the decision was made to include a product of weights with thresholds on family interactions.

Type of file: table
Label: SupTab1
Filename: Supplementary Table 1.doc

**Supplementary Table 1: Verified True Positive and True Negative microRNA targets in *C. elegans*.**

| Positive microRNA Targets | Negative microRNA Targets |
|---|---|
| *lin-4::lin-14* [1] | *lsy-6*::C02B8.4 |
| *lin-4::lin-28* [2] | *lsy-6*::C27H6.3 |
| *let-7::hbl-1* [3] | *lsy-6*::C48D5.2 |
| *let-7::lin-41* [4*] | *lsy-6*::F40H3.4 |
| *let-7::let-60* [5] | *lsy-6*::F55G1.12 |
| *let-7::daf-12* [6] | *lsy-6*::F59A6.1 |
| *let-7::pha-4* [6*] | *lsy-6*::R07E3.5 |
| *let-7::lss-4* [6] | *lsy-6*::T04C9.2 |
| *let-7::die-1* [6] | *lsy-6*::T05C12.8 |
| *let-7::nhr-23* [7] | *lsy-6*::T14G12.2 |
| *let-7::nhr-25* [7] | *lsy-6*::T20G5.9 |
| *let-7*::T14B1.1 [8] | *lsy-6*::T23E1.1 |
| *lsy-6::cog-1* [9*] | *lsy-6*::ZK637.13 |
| *mir-61::vav-1* [10*] | |
| *mir-273::die-1* [11#] | |

**Supplementary Table 1: Verified True Positive and True Negative microRNA targets in *C. elegans*.** Individual miRNA::target relationships identified in C. elegans by genetic or reporter assays. True positives are referenced in the table. True negatives were identified in a single study[12]. Asterisks (*) next to references refer to targets not identified by the AIN-IP method. [#] This microRNA is not conserved to C. briggsae, and so targets will not be found by mirWIP.

**References for Supplementary Table 1**


1 Lee, R. C., Feinbaum, R. L., and Ambros, V., The C. elegans heterochronic gene lin-4 encodes small RNAs with antisense complementarity to lin-14. *Cell* **75** (5), 843 (1993).

2 Moss, E. G., Lee, R. C., and Ambros, V., The cold shock domain protein LIN-28 controls developmental timing in C. elegans and is regulated by the lin-4 RNA. *Cell* **88** (5), 637 (1997).

3 Abrahante, J. E. et al., The Caenorhabditis elegans hunchback-like gene lin-57/hbl-1 controls developmental time and is regulated by microRNAs. *Dev Cell* **4** (5), 625 (2003).

4 Reinhart, B. J. et al., The 21-nucleotide let-7 RNA regulates developmental timing in Caenorhabditis elegans. *Nature* **403** (6772), 901 (2000).

5 Johnson, S. M. et al., RAS is regulated by the let-7 microRNA family. *Cell* **120** (5), 635 (2005).

[6] Grosshans, H. et al., The temporal patterning microRNA let-7 regulates several transcription factors at the larval to adult transition in C. elegans. *Dev Cell* **8** (3), 321 (2005).

[7] Hayes, G. D., Frand, A. R., and Ruvkun, G., The mir-84 and let-7 paralogous microRNA genes of Caenorhabditis elegans direct the cessation of molting via the conserved nuclear hormone receptors NHR-23 and NHR-25. *Development* **133** (23), 4631 (2006).

[8] Lall, S. et al., A genome-wide map of conserved microRNA targets in C. elegans. *Curr Biol* **16** (5), 460 (2006).

[9] Johnston, R. J. and Hobert, O., A microRNA controlling left/right neuronal asymmetry in Caenorhabditis elegans. *Nature* **426** (6968), 845 (2003).

[10] Yoo, A. S. and Greenwald, I., LIN-12/Notch activation leads to microRNA-mediated down-regulation of Vav in C. elegans. *Science* **310** (5752), 1330 (2005).

[11] Chang, S. et al., MicroRNAs act sequentially and asymmetrically to control chemosensory laterality in the nematode. *Nature* **430** (7001), 785 (2004).

[12] Didiano, D. and Hobert, O., Perfect seed pairing is not a generally reliable predictor for miRNA-target interactions. *Nat Struct Mol Biol* **13** (9), 849 (2006).